Above-threshold ionization in molecules by intense multiple-frequency circularly polarized laser pulses

Kai-Jun Yuan* and André D. Bandrauk†

Laboratoire de Chimie Théorique, Faculté des Sciences, Université de Sherbrooke, Sherbrooke, Québec, Canada J1K 2R1

(Received 3 May 2018; published 15 August 2018)

We present molecular above-threshold ionization (ATI) by multiple-frequency circularly polarized laser pulses. Simulations are performed on aligned H_2^+ by numerically solving corresponding time-dependent Schrödinger equations. Molecular ATI spectra show maximum cutoff and multiple ionization trajectories which depend on the pulse frequency combination. We describe the laser-induced electron dynamics by multiple frequency circularly polarized pulses in a rotating frame where the total ponderomotive energy of electrons is defined by the average frequency of the pulses. The influence of Coriolis effects in the photoionization is also studied. The present results illustrate the dependence of molecular photoionization on the pulse frequency combination and helicity, thus allowing for the control of circular-polarization electron dynamics in the more complex molecular systems.

DOI: 10.1103/PhysRevA.98.023413

I. INTRODUCTION

Following rapid developments in laser technology, numerous novel high-order nonlinear optical phenomena in the field of light-matter interaction have been studied widely [1,2]. Ultrashort laser pulses have led to photoimaging techniques such as laser Coulomb explosion for nuclear motion [3,4] to laser-induced electron diffraction (LIED) for coupled electron-nuclear motion [5,6]. Electrons have great potential for probing the time-resolved transient structure of molecules, materials, and even biological systems via ultrafast electron diffraction [7] due to their large scattering cross sections. In these schemes, a laser-induced rescattering mechanism occurs through recombination with the parent ion [8,9] with linear polarization electron wavelengths controlled by the laser intensity through laser-induced ponderomotive energies $U_p = e^2E_0^2/4m_e\omega^2$ for electric-field amplitude E_0, corresponding to an intensity $I_0 = c\epsilon_0 E_0^2/2$ and frequency ω.

Above-threshold ionization (ATI) [10] in atomic and molecular systems as one of the most fundamental strong-field phenomena has attracted considerable attention in both experimental and theoretical studies. In general a cutoff of energy $2U_p$ is produced in the ATI spectra [11]. For linear polarization, electron rescattering trajectories also make a considerable contribution to the ATI energy spectra [12–15]. Laser-induced electron recollision and rescattering leads to the maximum energy up to $10U_p$ [16,17]. An important application of ATI spectra in strong-field physics has been the imaging of electron orbitals using recolliding electrons by LIED [5,6,18] and, recently, by photoelectron holography [19,20]. For circular polarization processes, the electron recollision dynamics was shown to be suppressed by single circularly polarized pulses as early as 1989 with CO_2 lasers [11] and confirmed by a classical model [9] for atoms. We have shown that, in stretched molecules, an extension of ATI can be obtained with energies up to $32U_p$ due to laser-induced electron collisions with neighboring ions [21]. The interference between the direct liberated electrons and those scattered by neighboring ions can also produce the phenomenon of photoelectron holography in molecules [22]. Recently, ATI of rare-gas atoms by a bicircular field has been theoretically investigated by means of improved strong-field-approximation (SFA) methods [23] and confirmed experimentally by using a velocity map imaging photoelectron spectrometer and tomographic reconstruction techniques [24,25]. The enhancement of electron recollision with parent ions by intense counter-rotating bichromatic circularly polarized femtosecond pulses was predicted as early as 1995 [26–29], and is now a main source of circularly polarized high-order harmonic generation [30–37]. As a consequence of electron interference between the forward-scattered and nonscattered trajectories, multiple holographic patterns are observed in ATI momentum distributions [38], thus providing a way to image molecular structure.

The study of laser-induced electron dynamics by multiple frequency circularly polarized laser pulses is of great interest in, for example, electron vortices [39–43], ultrafast magnetic fields [44], and circular chiral dichroism [45–47]. However, it still remains difficult to exactly describe the laser-induced electron dynamics in photoionization processes. In the present work we focus on molecular ATI processes by multiple-frequency circularly polarized laser pulses. The molecular ion H_2^+ is used as a benchmark system to describe the circular polarization electron dynamics. Results are obtained from numerical solutions of the corresponding time-dependent Schrödinger equation (TDSE). Molecular and atomic ATI spectra have been well established both experimentally and theoretically, and many numerical methods have been suggested, including the closed-form analytic formulas [48]. From the numerical simulations we find that ATI spectra show maximum cutoff energies which can be described well by the laser-induced electron dynamics in a rotating frame [26,27].

*kaijun.yuan@usherbrooke.ca
†andre.bandrauk@usherbrooke.ca

The effects of light helicity, i.e., Coriolis effects, and pulse phases are also presented.

The paper is arranged as follows: in Sec. II, we briefly describe the numerical and computational methods. Simulation results obtained by time-dependent quantum electron wave-packet calculations from the corresponding TDSE for aligned H_2^+ are presented and discussed in Sec. III. We analyze such molecular ATI spectra based on laser-induced electron dynamics in a rotating frame. Finally, we summarize our findings in Sec. IV. Throughout this paper, atomic units (a.u.) are used unless otherwise noted.

II. NUMERICAL AND COMPUTATIONAL METHODS

To simulate ATI spectra in molecules with multiple-frequency circularly polarized laser fields, we numerically solve the corresponding TDSE for the aligned molecule H_2^+ within a static nuclear (Born–Oppenheimer approximation) frame,

$$i\frac{\partial}{\partial t}\psi(\mathbf{r},t) = H(\mathbf{r},t)\psi(\mathbf{r},t), \tag{1}$$

with the field-molecule Hamiltonian $H(\mathbf{r},t) = H_0(\mathbf{r}) + H_L(\mathbf{r},t)$. $H_0(\mathbf{r}) = T(\mathbf{r}) + V_c(\mathbf{r})$, where $T(\mathbf{r})$ is the kinetic operator and $V_c(\mathbf{r})$ is the molecular two-center Coulomb potential. $H_L(\mathbf{r},t) = \mathbf{r}\cdot\mathbf{E}$ is the field-molecule interaction term which is described in the length gauge. The electron dynamics is described in the polar coordinates $\mathbf{r} = (x, y) = (\rho\cos\theta, \rho\sin\theta)$ [49]. Then the corresponding kinetic operator $T(\rho,\theta)$ is given by

$$T(\rho,\theta) = -\frac{1}{2}\left(\frac{1}{\rho}\frac{\partial}{\partial\rho}\rho\frac{\partial}{\partial\rho} + \frac{1}{\rho^2}\frac{\partial^2}{\partial^2\theta}\right). \tag{2}$$

We solve the TDSE in Eq. (1) by using a second-order-accurate split-operator method with time step δt and combined with a fifth-order finite difference method and Fourier transform technique in the spatial steps $\delta\rho$ and $\delta\theta$ [50]. The time step is taken to be $\delta t = 0.01$ a.u. $= 0.24$ as. The spatial discretization is $\delta\rho = 0.25$ a.u. for a radial grid range $0 \leqslant \rho \leqslant 1024$ a.u. and the angle grid size $\delta\theta = 0.025$ radian. To prevent unphysical effects due to the reflection of the electron wave packet from the boundary, we multiply $\psi(\rho,\theta,t)$ at each time step by a "mask function" or absorber with the form $g(t) = \cos^{1/8}[\pi(\rho-\rho_a)/2\rho_{abs}]$, $\rho_a \leqslant \rho \leqslant \rho_{\max}$. For all results reported here we set the absorber domain $\rho_a = \rho_{\max} - \rho_{abs} = 896$ a.u. with $\rho_{abs} = 128$ a.u.

Molecular photoelectron distributions (i.e., ATI spectra) are calculated by a Fourier transform of the time-dependent electronic wave function $\psi(\rho,\theta,t)$ in Eq. (1), which exactly describes the electron dynamics in the continuum [51]:

$$\begin{aligned}
\mathcal{J}_l(\theta,E)|_{\rho_f} &= \int_{t_p}^{\infty}\psi(\theta,t)|_{\rho_f}e^{iEt}dt,\\
\mathcal{J}_r(\theta,E)|_{\rho_f} &= \int_{t_p}^{\infty}\left.\frac{\partial\psi(\theta,t)}{\partial\rho}\right|_{\rho_f}e^{iEt}dt,\\
\mathcal{J}(\theta,E) &\sim \mathrm{Re}\left[\frac{1}{2i}\mathcal{J}_l^*(\theta,E)|_{\rho_f}\mathcal{J}_r(\theta,E)|_{\rho_f}\right],
\end{aligned} \tag{3}$$

where t_p is the time after the pulse turns off and $\rho_f = 890$ a.u. is an asymptotic point before the wave packet is absorbed. $E = p_e^2/2$ is the kinetic energy of an ionized electron with wave vector $k = p_e = 2\pi/\lambda_e$, and $p_e = (p_x^2 + p_y^2)^{1/2}$ is the momentum of a photoelectron of wavelength λ_e. ATI energy spectra are obtained by integrating over the angle,

$$\mathcal{J}(E) = \int d\theta\mathcal{J}(\theta,E). \tag{4}$$

III. RESULTS AND DISCUSSIONS

The purpose of the present work is to study molecular ATI spectra and electron dynamics by multiple-frequency circularly polarized laser pulses. We use the hydrogen molecular ion H_2^+ as a benchmark system which can be fully investigated in theory and experiment [52]. The molecule H_2^+ is aligned along the x axis and the circularly polarized laser pulse with its field vector polarized in the (x, y) plane propagates along the z axis. The ATI spectra obtained from Eq. (4) reflect the laser-induced electron dynamics in the circularly polarized pulse. We derive equations of electron motion for circular polarization ionization in a rotating frame to understand these ATI phenomena. For H_2^+ the molecular vibrational and rotational periods on femtosecond (10^{-15} s) and picosecond (10^{-12} s) timescales are larger than that of the electron motion on attosecond (10^{-18} s) timescales. Therefore, the frozen nuclei calculation is valid for describing the ultrafast electron dynamics by ultrashort laser pulses.

A. Above-threshold-ionization spectra by bichromatic (ω_1, ω_2) circularly polarized laser pulses

We first consider the cases of molecular photoionization by bichromatic circularly polarized laser pulses. To understand the ATI process in bichromatic circularly polarized laser fields, we describe the laser-induced electron dynamics in a rotating frame. Modulation of the envelope at frequency ω of a single circularly polarized pulse of frequency $\bar{\omega}$ in the (x, y) plane is represented by the radiative, laser-matter, Hamiltonian H_L,

$$\begin{aligned}
H_L(t) &= 2E_0\cos(\omega t)[x\cos(\bar{\omega}t) + y\sin(\bar{\omega}t)]\\
&= E_0\{x\cos[(\omega+\bar{\omega})t] + y\sin[(\omega+\bar{\omega})t]\}\\
&\quad + E_0\{x\cos[(\omega-\bar{\omega})t] - y\sin[(\omega-\bar{\omega})t]\}.
\end{aligned} \tag{5}$$

$H_0(\mathbf{r})$ is a field-free static nuclei (Born–Oppenheimer) Hamiltonian. Equation (5) demonstrates that a single circularly polarized pulse of frequency $\bar{\omega}$ with an envelope modulated at frequency ω corresponds to two independent circularly polarized pulses of frequencies $\omega_1 = \omega + \bar{\omega}$ and $\omega_2 = \omega - \bar{\omega}$, rotating in the (x, y) molecular plane. For modulation frequencies $\omega > \bar{\omega}$ ($\omega_2 > 0$) one has two *counter-rotating* (opposite helicity) pulses whereas for $\omega < \bar{\omega}$ ($\omega_2 < 0$), Eq. (5) represents two *corotating* (same helicity) pulses. Applying the unitary transformation $\mathcal{T} = \exp(i\bar{\omega}tl_z)$, a rotation in the (x, y) molecular plane around the perpendicular z propagation direction gives the new Hamiltonian at the rotating frequency $\bar{\omega} = (\omega_1 - \omega_2)/2$ with the mean frequency $\omega = (\omega_1 + \omega_2)/2$ [26,27,31,53,54],

$$H' = H_0' + \bar{\omega}l_z + 2xE_0\cos(\omega t). \tag{6}$$

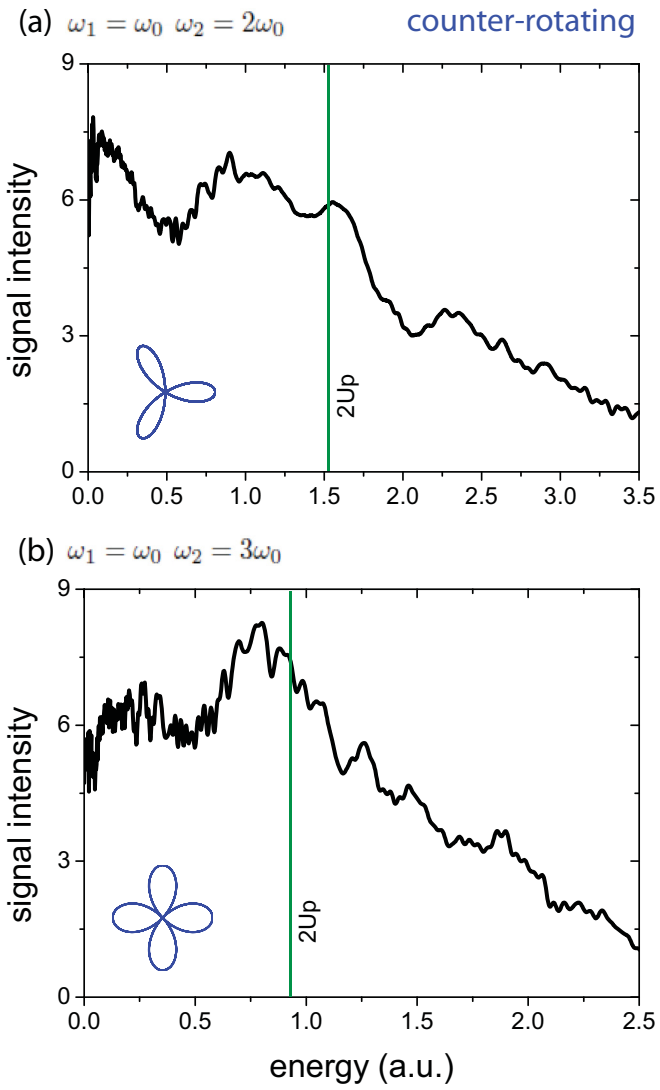

FIG. 1. ATI energy spectra in the molecule H_2^+ aligned along the x axis by bichromatic counter-rotating circularly polarized laser pulses at frequencies (a) $\omega_1 = \omega_0$ and $\omega_2 = 2\omega_0$ ($\omega = 3\omega_0/2$) and (b) $\omega_1 = \omega_0$ and $\omega_2 = 3\omega_0$ ($\omega = 2\omega_0$), where $\omega_0 = 0.057$ a.u., corresponding to $\lambda_0 = 800$ nm. The intensity and duration are $I_0 = 2\times10^{14}$ W/cm^2 ($E_0 = 0.0755$ a.u.) and $T = 21.15$ fs. Vertical lines indicate the ATI energies at $2U_p$, where the ponderomotive energy defines $U_p = (2E_0)^2/4\omega^2$, with the average frequency $\omega = (\omega_1 + \omega_2)/2$. Arbitrary units in ATI spectra are used.

Equation (6) shows generally that coplanar bichromatic circular pulses in the rotating frame $\bar{\omega}$ correspond to a linear driving-field term $2xE_0\cos(\omega t)$ in competition with a rotation angular-momentum term $+\omega l_z$ (around the z axis) responsible for Coriolis forces. The laser-driving term in Eq. (6) couples different angular-momentum terms, thus also pumping energy into circular current motion. One therefore predicts that the maximum ATI spectra appear at energies $2U_p$, where $U_p = (2E_0)^2/4\omega$ is the ponderomotive energy.

In Fig. 1 we display simulation results of ATI spectra in the molecule H_2^+ aligned along the x axis by bichromatic counter-rotating circularly polarized laser pulses, i.e., $\omega > \bar{\omega}$ in Eq. (6). The form of the driving laser pulse reads

$$\begin{aligned}\mathbf{E}(t) &= \mathbf{E}_1(t) + \mathbf{E}_2(t)\\ &= E_0 f(t)\{\hat{e}_x[\cos(\omega_1 t) + \cos(\omega_2 t)]\\ &\quad + \hat{e}_y[\sin(\omega_1 t) - \sin(\omega_2 t)]\}. \end{aligned} \tag{7}$$

$\hat{e}_{x/y}$ are the laser polarization directions and ω_1 and ω_2 are pulse frequencies. A trapezoid envelope $f(t)$ for a duration of $T = 8\tau = 21.15$ fs, where $1\tau = 2\pi/\omega_0$, with two-cycle rise and fall is used. $E_0 = 0.0755$ a.u. is the maximum amplitude of the field, corresponding to the pulse intensity $I_0 = 2\times10^{14}$ W/cm^2. Two frequency combinations $\omega_1 = \omega_0$ and $\omega_2 = 2\omega_0$ [Fig. 1(a)] and $\omega_1 = \omega_0$ and $\omega_2 = 3\omega_0$ [Fig. 1(b)], where $\omega_0 = 0.057$ a.u. servers as a fundamental frequency, corresponding to $\lambda_0 = 800$ nm, are used to simulate molecular ATI spectra. The H_2^+ molecular ion is prepared initially in the ground $1s\sigma_g$ electronic state and its eigenfunction is obtained by an imaginary-time-propagation method using the zero-field TDSE in Eq. (1).

From Fig. 1 we see that the maxima of ATI spectra occur at energies 1.56 a.u. at $\omega_1 = \omega_0$ and $\omega_2 = 2\omega_0$ [Fig. 1(a)] and 0.9 a.u. at $\omega_1 = \omega_0$ and $\omega_2 = 3\omega_0$ [Fig. 1(b)], corresponding to $2U_p$ with the average frequency $\omega = (\omega_1 + \omega_2)/2$ predicted in Eq. (6) (vertical green lines in Fig. 1). This cutoff energy results from the direct ionization process. We confirm these results from a quasiclassical laser-induced ionization model of an electron moving in the rotating frame by a linear driving laser field $2E_0\cos(\omega t)$ in Eq. (6). The corresponding induced electron velocity reads

$$\dot{x}(t) = -\frac{2E_0}{\omega}[\sin(\omega t) - \sin(\omega t_0)], \tag{8}$$

where t_0 is the ionization (birth) time of the liberated electron. From Eq. (8) one then obtains that the cutoff energy $2U_p$ occurs at $t_0 = 0$ and $t = (n + 1/2)\pi/\omega, n = 0, \pm1, \pm2, \pm3, \ldots$, where $x(t_0 = 0) = 0$. The corresponding rotation angle $\bar{\omega}t = \pi/6$ indicates that, during the ionization process, the electron lies mainly along the linear x polarization direction and the Coriolis effect is negligible. After the energies $2U_p$, ATI spectra decrease in amplitude. From Eq. (8) the maximum kinetic energy $\dot{x}^2(t)/2 = 8U_p$ should be predicted at $\omega t - \omega t_0 = (2n + 1)\pi$, which however cannot occur for laser pulses because the electron is ionized via tunneling since the electric field at the initial phase $\omega t_0 = \pi/2$ is zero and the tunneling probability is zero as well.

In Fig. 2 we display angle- and energy-resolved ATI spectra by bichromatic circularly polarized laser pulses with the two frequency combinations $\omega_1 = \omega_0$ and $\omega_1 = 2\omega_0$ ($\omega = 3\omega_0/2$) [Fig. 2(a)] and $\omega_1 = \omega_0$ and $\omega_1 = 3\omega_0$ ($\omega = 2\omega_0$) [Fig. 2(b)]. It is found that various ionization trajectories are produced. At $\omega_1 = \omega_0$ and $\omega_2 = 2\omega_0$ ($\omega = 3\omega_0/2$) three ionization trajectories appear at about angles 45°, 155°, and 285° whereas at $\omega_1 = \omega_0$ and $\omega_2 = 3\omega_0$ four ionization trajectories are produced at about angles 30°, 120°, 210°, and 300°. The ATI spectra show K ionization trajectories with angle intervals $2\pi/K$, where $K = k_1 + k_2$ and $\omega_1/\omega_2 = k_1/k_2$. The ionization trajectories illustrate the symmetry of the net laser fields. The electric field in Eq. (7) is $2\pi k_1/\omega_1$ time periodic and exhibits a K-fold

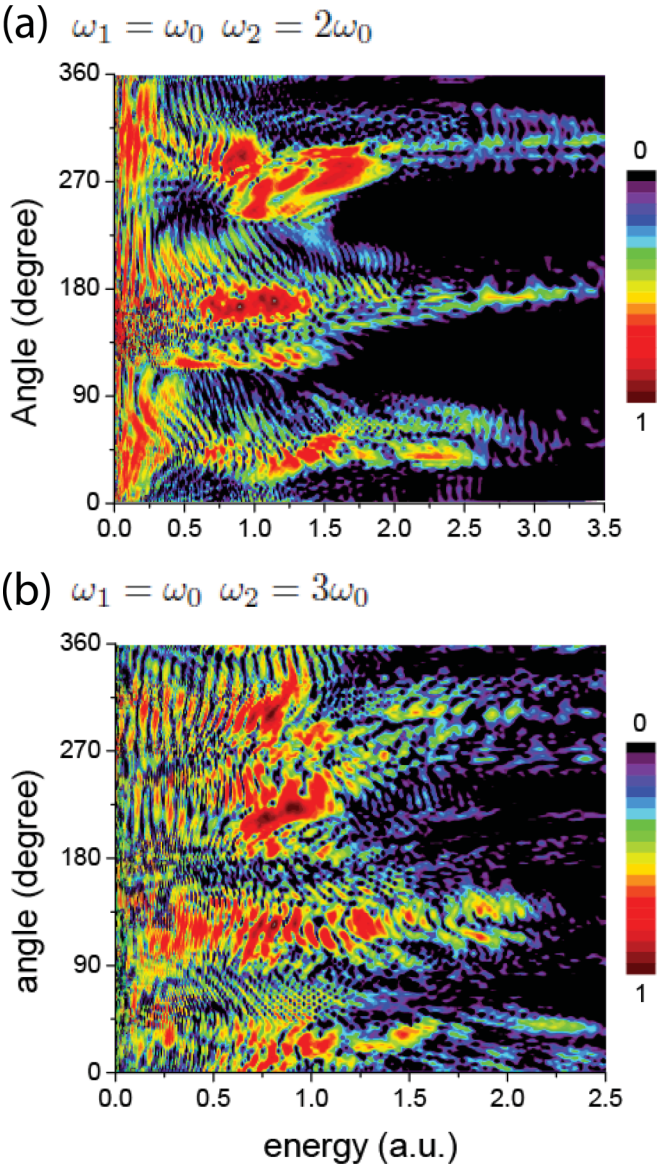

FIG. 2. Angle- and energy-resolved ATI spectra in the molecule H_2^+ aligned along the x axis by bichromatic counter-rotating circularly polarized laser pulses at frequencies (a) $\omega_1 = \omega_0$ and $\omega_2 = 2\omega_0$ ($\omega = 3\omega_0/2$) and (b) $\omega_1 = \omega_0$ and $\omega_2 = 3\omega_0$ ($\omega = 2\omega_0$), $\omega_0 = 0.057$ a.u. corresponding to $\lambda_0 = 800$ nm. The intensity and duration are $I_0 = 2\times10^{14}$ W/cm^2 and $T = 21.15$ fs. Arbitrary units in ATI distributions are used.

symmetry,

$$E(t + n\Theta/\omega_1) = \Omega(n\Theta)E(t), \tag{9}$$

where $\Theta = 2k_1\pi/K$ and $\Omega(n\Theta)$ is the rotation matrix around the z axis with angle $n\Theta$. That leads to three- and fourfold symmetries for the $\omega_1/\omega_2 = 1/2$ and $\omega_1/\omega_2 = 1/3$ fields. The total molecule-field Hamiltonian also presents K-fold symmetry. The ionization repeats itself over time, following a similar symmetry as the fields in Eq. (9). Therefore, the angular nodes of the ionization trajectories illustrate the symmetry fold of the net laser fields.

The bichromatic circularly polarized laser pulses with counter-rotating components can also lead to electron recollision with the parent ions. When a recolliding electron is backscattered by the parent ions in the field in Eq. (6), its velocity becomes

$$\dot{x}(t) = \frac{2E_0}{\omega}[\sin(\omega t - \omega t_{rc}) + \sin(\omega t_{rc} + \omega t_0) + \sin(\omega t_0)], \tag{10}$$

for $t > t_{rc}$. t_{rc} is the recollision time of electrons with the parent ion, and the corresponding maximum kinetic energy is $\dot{x}^2(t_{rc})/2 = 3.17U_p$. From Eq. (10) the corresponding asymptotic energy of the ionized electron is $\dot{x}^2(t)/2 = 10.2U_p$ [16,17]. Of note is that, due to Coriolis effects, these electron recollision and rescattering trajectories rotate far from the laser polarization x direction. As a result, the ionization is suppressed by molecular Coulomb effects and the ATI spectral intensity with high energies is very weak.

In the counter-rotating cases in Figs. 1 and 2 the rotating frequency $\bar{\omega} = (\omega_2 - \omega_1)/2$ is smaller than the average frequency $\omega = (\omega_1 + \omega_2)/2$. We next compare the results of ATI processes by a bichromatic corotating circularly polarized laser pulse, i.e., $\bar{\omega} > \omega$ in Eq. (6). The form of the laser pulse is given by

$$\begin{aligned}\mathbf{E}(t) &= \mathbf{E}_1(t) + \mathbf{E}_2(t) \\ &= E_0 f(t)\{\hat{e}_x[\cos(\omega_1 t) + \cos(\omega_2 t)] \\ &\quad + \hat{e}_y[\sin(\omega_1 t) + \sin(\omega_2 t)]\}.\end{aligned} \tag{11}$$

Figure 3 displays the corresponding ATI spectra in the molecule H_2^+ aligned along the x axis. The laser parameters are the same as in Fig. 1, except with corotating components. For the case in Eq. (11), the rotating frequency in Eq. (6) is $\bar{\omega} = (\omega_1 + \omega_2)/2$ and the mean frequency of the linearly polarized driving field is $\omega = (\omega_2 - \omega_1)/2$. At frequencies $\omega_1/\omega_2 = 1/2$ and $1/3$, the corresponding cutoff energies should be predicted at $2U_p = 14.05$ a.u. and 3.5 a.u., where $U_p = (2E_0)^2/4\omega^2$, by Eq. (6). However, as shown in Fig. 3 the corresponding results obtained from numerical simulations are respectively 3.4 a.u. and 1.75 a.u., smaller than those predictions in Eq. (6). The difference indicates the importance of the Coriolis effects.

In the corotating component cases in Fig. 3, the rotating frequency is lager than the mean frequency, $\bar{\omega} > \omega$. The Coriolis force leads to the electron far from the polarization direction of the linearly driving field in Eq. (6). As a result, the ATI spectra are suppressed. The ATI energy spectra in Fig. 3 mainly arise from the liberated electron along the x polarization direction. During the ionization, the electron is driven by the field $2E_0\cos(\omega t)$. The maximum kinetic energy should occur at $t = \pi/2\bar{\omega}$, where the rotation angle $\bar{\omega}t = \pi/2$, perpendicular to the laser x polarization direction. As predicted by Eq. (8), the corresponding maximum energy gives $\dot{x}^2(t)/2 = 2E_0^2\sin^2(\omega t)/\omega^2$. For the cases at frequencies $\omega_1/\omega_2 = 1/2$, the corresponding maximum energy is $U_p/2 = 3.5$ a.u. and $U_p = 1.75$ a.u. at frequencies $\omega_1/\omega_2 = 1/3$. The simulations from numerical calculations agree with very well the theoretical predictions in Eq. (8) from the classical model in a rotating frame. The suppression of ionization in Fig. 3 with the corotating components reflects essentially the effects of the Coriolis force, i.e., $\bar{\omega}l_z$, in the ATI processes.

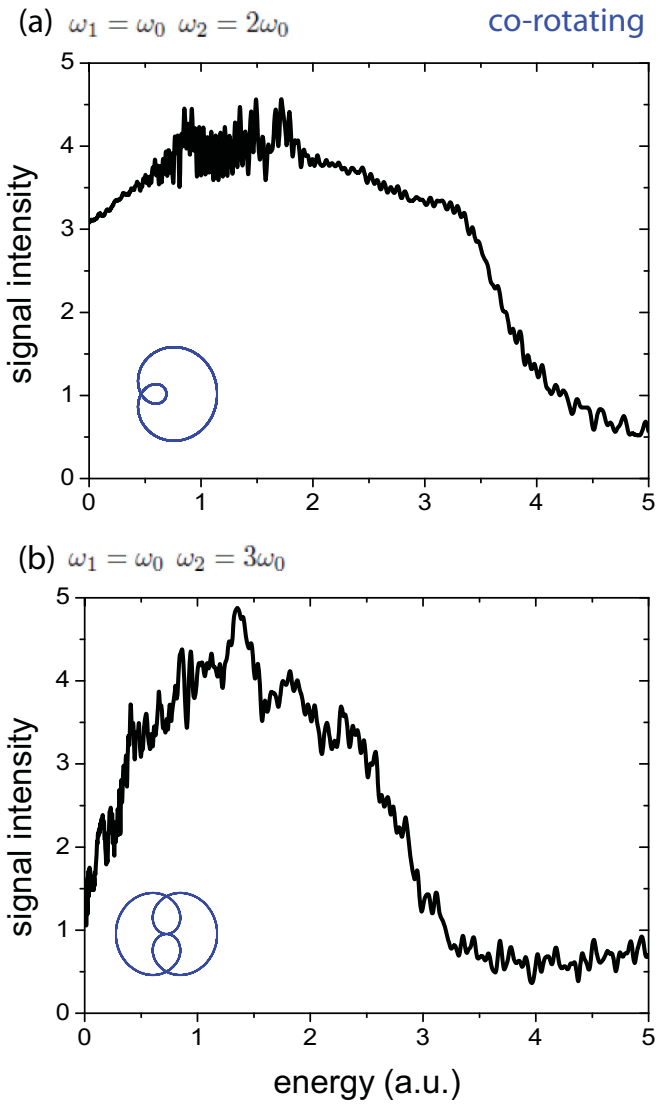

FIG. 3. ATI energy spectra in the molecule H_2^+ aligned along the x axis by bichromatic corotating circularly polarized laser pulses at frequencies (a) $\omega_1 = \omega_0$ and $\omega_2 = 2\omega_0$ ($\omega = 3\omega_0/2$) and (b) $\omega_1 = \omega_0$ and $\omega_2 = 3\omega_0$ ($\omega = 2\omega_0$), with $\omega_0 = 0.057$ a.u. corresponding to 800 nm. The intensity and duration are $I_0 = 2\times10^{14}$ W/cm^2 and $T = 21.15$ fs. The insets show the field vectors. Arbitrary units in ATI spectra are used.

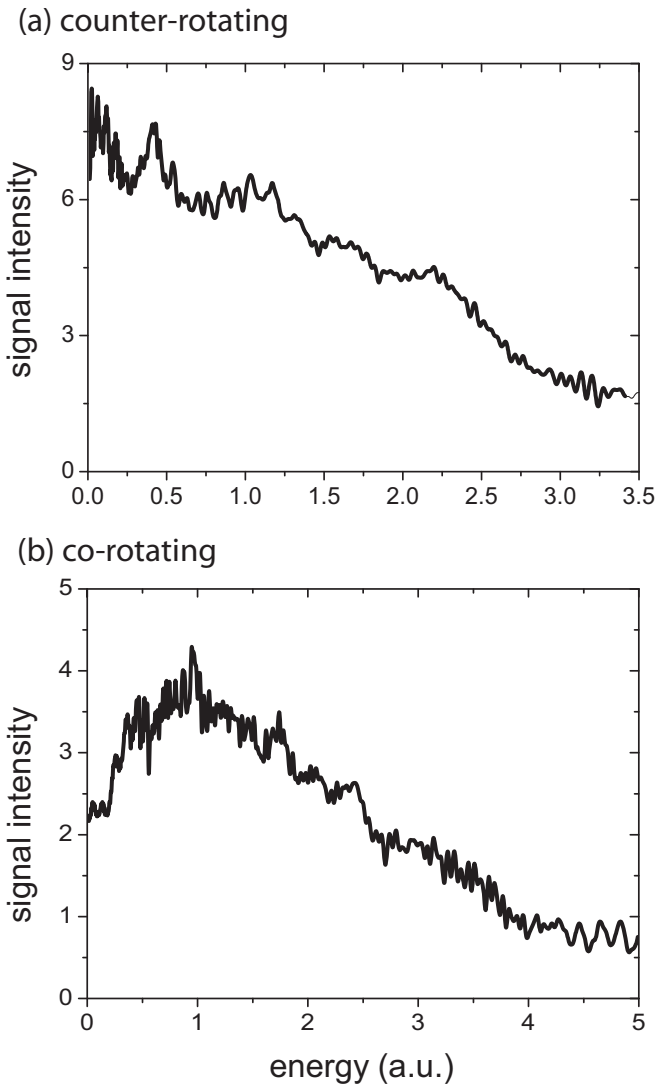

FIG. 4. ATI energy spectra in the atom H by bichromatic $\omega_1 = \omega_0$ and $\omega_2 = 2\omega_0$ circularly polarized laser pulses with (a) counter-rotating component, $\bar{\omega} = (\omega_1 - \omega_2)/2$ and $\omega = (\omega_1 + \omega_2)/2$, and (b) corotating component, $\bar{\omega} = (\omega_1 + \omega_2)/2$ and and $\omega = (\omega_1 - \omega_2)/2$. The intensity and duration are $I_0 = 2\times10^{14}$ W/cm^2 ($E_0 = 0.0755$ a.u.) and $T = 21.15$ fs. Arbitrary units in ATI spectra are used.

For comparison, we also present the ATI process of the atom H. Figure 4 shows ATI energy spectra produced by bichromatic $\omega_1 = \omega_0$ and $\omega_2 = 2\omega_0$ circularly polarized pulses with counter-rotating [Fig. 4(a)] and corotating [Fig. 4(b)] components. The other laser parameters are the same as those used in Figs. 1–3. It is found that similar results are produced for both counter-rotating and corotating processes, as for H_2^+ in Figs. 1(a) and 3(a). The ATI energy spectra of H_2^+ and H show the maxima with the same kinetic energies, which reflects the similar circular polarization electron trajectories by the laser fields. After tunneling ionization, the liberated electron does not significantly interact with the parent ion. Of note is that we focus here on the low-order ATI spectra, i.e., the electron is released directly from the atomic and molecular centers. However, the liberated electron can also be driven back to the parent ion, leading to high kinetic energies, as predicted by Eq. (10). The rescattering electron that encodes the structural information of the parent ions [55] therefore provides insight into the coherent electron dynamics [56,57].

B. Four-frequency circular polarization above-threshold-ionization processes

We present ATI processes in four-color circularly polarized laser fields at different frequencies with the form

$$\begin{aligned}\mathbf{E}(t) &= \mathbf{E}_1(t) + \mathbf{E}_2(t) + \mathbf{E}_3(t) + \mathbf{E}_4(t)\\ &= E_0 f(t)\{\hat{e}_x[\cos(\omega_1 t + \phi_1) + \cos(\omega_2 t + \phi_2)\\ &\quad + \cos(\omega_3 t + \phi_3) + \cos(\omega_4 t + \phi_4)]\\ &\quad + \hat{e}_y[\sin(\omega_1 t + \phi_1) - \sin(\omega_2 t + \phi_2)\\ &\quad + \sin(\omega_3 t + \phi_3) - \sin(\omega_4 t + \phi_4)]\}. \qquad (12)\end{aligned}$$

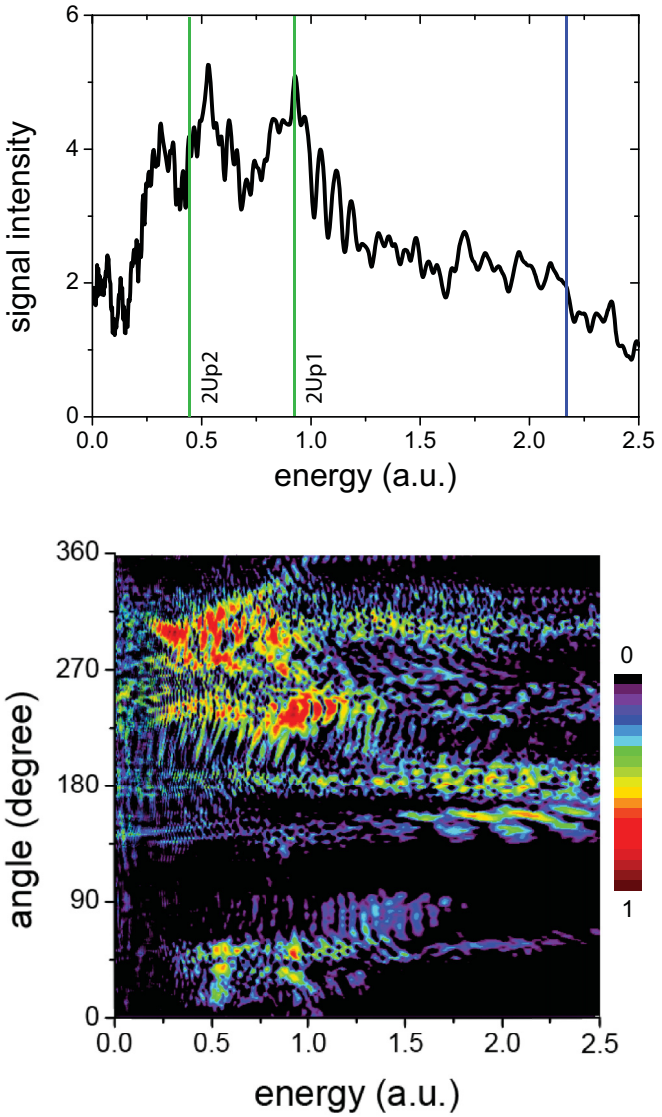

FIG. 5. (top) ATI energy spectra in the molecule H_2^+ aligned along the x axis by four-color circularly polarized laser pulses at frequencies $\omega_1 = \omega_0$, $\omega_2 = 3\omega_0$, $\omega_3 = 2\omega_0$, and $\omega_4 = 4\omega_0$, where $\omega_0 = 0.057$ a.u. corresponding to $\lambda_0 = 800$ nm. The intensity and duration are $I_0 = 2\times10^{14}$ W/cm^2 ($E_0 = 0.0755$ a.u.) and $T = 21.15$ fs. The CEPs are $\phi_n = 0$, $n = 1, 4$. Vertical lines indicate the ATI energies at $2U_{p1}$ and $2U_{p2}$ with $U_{p1} = (2E_0)^2/4\omega^2$, $\omega = (\omega_1 + \omega_2)/2$, and $U_{p2} = (2E_0)^2/4\omega'^2$, $\omega' = (\omega_3 + \omega_4)/2$. (bottom) The corresponding angular and energy resolved ATI spectra. Arbitrary units are used.

In Fig. 5 we show the numerical result of ATI spectra for the molecular ion H_2^+ aligned along the x axis by four-color circularly polarized laser pulses. The pulse frequencies are chosen as $\omega_1 = \omega_0$ (wavelength $\lambda_1 = 800$ nm), $\omega_2 = 3\omega_0$ ($\lambda_2 = 266.7$ nm), $\omega_3 = 2\omega_0$ ($\lambda_3 = 400$ nm), and $\omega_4 = 4\omega_0$ ($\lambda_4 = 200$ nm), where $\omega_0 = 0.057$ a.u. ($\lambda_0 = 800$ nm) is the fundamental frequency. The pulse intensity $I_0 = 2\times10^{14}$ W/cm^2 ($E_0 = 0.0755$ a.u.) and duration $T = 21.15$ fs are fixed. The carrier envelope phases (CEPs) ϕ_n, $n = 1, 4$ are always set as zero. Results show that two maximum peaks are generated at energies 0.5 a.u. and 0.9 a.u. It is also found that the ionization trajectories are strongly asymmetric. The photoelectron is mainly localized around the angles $270^\circ \pm 20^\circ$.

The multiple frequency circular polarization ATI spectra in Fig. 5 are composed of double bichromatic circular polarization ionization processes. We next describe the four-color laser-induced electron dynamics in a rotating frame. In the presence of intense circularly polarized laser pulses with different frequency-modulated envelopes $f(t)\cos(\omega t)$ and $f(t)\cos(\omega' t)$, the field-molecule interaction Hamiltonian is given, in the length gauge, by

$$\begin{aligned} H_L(t) &= H_{L1}(t) + H_{L2}(t) \\ &= 2E_0 f(t)\cos(\omega t)[x\cos(\bar{\omega}t) + y\sin(\bar{\omega}t)] \\ &\quad + 2E_0 f(t)\cos(\omega' t)[x\cos(\bar{\omega}' t) + y\sin(\bar{\omega}' t)], \end{aligned} \tag{13}$$

where the two Hamiltonian terms are, respectively,

$$\begin{aligned} H_{L1}(t) &= \mathbf{r}\cdot[\mathbf{E}_1(t) + \mathbf{E}_2(t)] \\ &= E_0 f(t)\{x\cos[(\omega+\bar{\omega})t] + y\sin[(\omega+\bar{\omega})t]\} \\ &\quad + E_0 f(t)\{x\cos[(\omega-\bar{\omega})t] - y\sin[(\omega-\bar{\omega})t]\}, \end{aligned} \tag{14}$$

and

$$\begin{aligned} H_{L2}(t) &= \mathbf{r}\cdot[\mathbf{E}_3(t) + \mathbf{E}_4(t)] \\ &= E_0 f(t)\{x\cos[(\omega'+\bar{\omega}')t] + y\sin[(\omega'+\bar{\omega}')t]\} \\ &\quad + E_0 f(t)\{x\cos[(\omega'-\bar{\omega}')t] - y\sin[(\omega'-\bar{\omega}')t]\}. \end{aligned} \tag{15}$$

Equation (13) demonstrates that two single circularly polarized pulses of frequencies $\bar{\omega}$ and $\bar{\omega}'$ with envelopes $f(t)\cos(\omega t)$ and $f(t)\cos(\omega' t)$ modulated at frequencies ω and ω' correspond to four independent circularly polarized pulses of frequencies ($\omega_1 = \omega - \bar{\omega}$, $\omega_2 = \omega + \bar{\omega}$) and ($\omega_3 = \omega' - \bar{\omega}'$, $\omega_4 = \omega' + \bar{\omega}'$) rotating in the (x, y) molecular plane. Applying the unitary transformation $\mathcal{T} = \exp[i(\bar{\omega} + \bar{\omega}')tl_z/2]$, a rotation in the (x, y) molecular plane around the perpendicular z propagation direction gives the Hamiltonian

$$\begin{aligned} H'_L(t) &= 2E_0 f(t)\cos(\omega t)\{x\cos[(\bar{\omega}-\bar{\omega}')t/2] \\ &\quad + y\sin[(\bar{\omega}-\bar{\omega}')t/2]\} + 2E_0 f(t)\cos(\omega' t) \\ &\quad \times\{x\cos[(\bar{\omega}-\bar{\omega}')t/2] - y\sin[(\bar{\omega}-\bar{\omega}')t/2]\}. \end{aligned} \tag{16}$$

Equation (16) corresponds to two pulses of opposite helicity at the frequency $\bar{\omega} - \bar{\omega}'$ and different modulations at frequencies ω and ω'. We consider the case with the same rotating frequencies of the two counter-rotating pulses at frequency combinations (ω_1, ω_2) and (ω_3, ω_4), i.e., $\bar{\omega} = \bar{\omega}'$. Then the radiative Hamiltonian in Eq. (16) reduces to two linearly polarized pulses,

$$H''_L = 2xE_0 f(t)[\cos(\omega t) + \cos(\omega' t)]. \tag{17}$$

Equation (17) shows generally that coplanar four-color ω_n, $n = 1, 4$, circularly polarized pulses in the rotating frame correspond to two linearly polarized driving-field terms $2xE_0 f(t)\cos(\omega t)$ and $2xE_0 f(t)\cos(\omega' t)$, in competition with a rotation angular momentum term $\bar{\omega}l_z$ or $\bar{\omega}'l_z$ (around the z

axis) responsible for Coriolis forces, which do not commute with each other because $l_z = -i[x\partial/\partial y - y\partial/\partial x]$.

From Eqs. (13)–(17) we note that the total pulse is composed of two counter-rotating circularly polarized pulse combinations, in Eqs. (14) and (15), i.e., a 800 nm and 266.7 nm combination with a fourfold symmetry and a 400 and 200 nm combination with a threefold symmetry. In the rotating frame, the two linearly polarized driving fields $2E_0 f(t)\cos(\omega t)$ and $2E_0 f(t)\cos(\omega' t)$ give rise to cutoffs of ATI spectra at energies $2U_{p1} = 0.88$ a.u. and $2U_{p2} = 0.39$ a.u., where $U_{p1} = (2E_0)^2/4\omega^2$, $\omega = (\omega_1 + \omega_2)/2$ and $U_{p2} = (2E_0)^2/4\omega'^2$, $\omega' = (\omega_3 + \omega_4)/2$. These values correspond to the two ATI peaks (green lines) in Fig. 5. Of note is that around the energy 2.2 a.u., a plateau of ATI spectra is produced as well. From Eq. (17), the corresponding laser-induced electron velocity is given by

$$\dot{x}(t) = -2E_0\left[\frac{\sin(\omega t) - \sin(\omega t_0)}{\omega} + \frac{\sin(\omega' t) - \sin(\omega' t_0)}{\omega'}\right]. \tag{18}$$

The ionization processes induced by the linearly x polarized field $2E_0 f(t)\cos(\omega t)$ are modulated by the second $2E_0 f(t)\cos(\omega' t)$ field. As predicted in Eq. (18), the two-color direction ionization gives rise to a maximum cutoff energy of $\dot{x}^2(t)/2 = 2.2$ a.u., where $t_0 = 0$ and $t = (2n \pm 0.2)\pi/\omega_0$. Therefore, the extension of the ATI cutoff spectrum is produced, as shown in Fig. 5 (blue line). Moreover, the two linearly x polarized driving fields $2E_0 f(t)\cos(\omega t)$ and $2E_0 f(t)\cos(\omega' t)$ in Eq. (17) lead to a asymmetric net field. Consequently, the total field-molecule Hamiltonian is not periodic. Since ionization trajectories follow the total field vector, asymmetric angular distributions of ATI are produced in Fig. 5(b).

In Fig. 6 we display ATI spectra at different relative phases ϕ by four-color circularly polarized laser pulses. The CEPs $\phi_1 = \phi_2 = 0$ are fixed and $\phi_3 = \phi_4$ are set at $\pi/2$ [Fig. 6(a)] and π [Fig. 6(b)], i.e., their relative phases are respectively $\phi = \pi/2$ and π. From Fig. 6 one sees that the ATI spectra are modulated by varying the relative phase ϕ between the two field components in Eqs. (14) and (15). At $\phi = \pi/2$ the ATI spectra around energies 1.5 a.u. are enhanced in amplitude, and at $\phi = \pi$ an extension of ATI spectra is obtained with energies 2.5 a.u. However, around the $2U_{p1}$ and $2U_{p2}$ cutoff energies, varying CEPs only gives rise to a slight variance of ATI spectral amplitudes. The enhancement of ATI spectra at high-energy regions illustrate the laser-induced electron dynamics. In the rotating frame, for the two linearly polarized fields, their relative phases will influence the ionization processes by steering tunneling electrons. The maximum energy of the electron wave packet is dependent on the CEP of the driving pulses, leading to a modulation of ATI spectra. Similar phenomena have been obtained in high-order harmonic spectra by multiple-color laser pulses; see, e.g., Refs. [58,59].

In the present work we simulate ATI spectra by solving TDSEs. Comparison of the results for the molecule H_2^+ and the atom H shows that Coulomb potentials play a minor role in the low-energy ($\leqslant 2U_p$) ionization process. The low-energy ATI spectra mainly result from direct ionization by the bichromatic circularly polarized laser pulses. The electron-ion rescattering process is therefore negligible. Such processes can also be reproduced by carrying out classical trajectory Monte Carlo (CTMC) numerical simulations [25] with and without Coulomb potentials. The ATI energy spectra reflect the classical trajectories of the liberated electron by the linearly polarized driving laser fields in the rotating frame. Of note is that, during the ionization processes, the subcycle interference effects of electron wave packets [19,20] can also lead to more complex structure in the photoelectron momentum distributions, as illustrated in Fig. 2. Such interference effects, however, are absence in the results of CTMC [25]. The interference patterns are shown to depend on the molecular

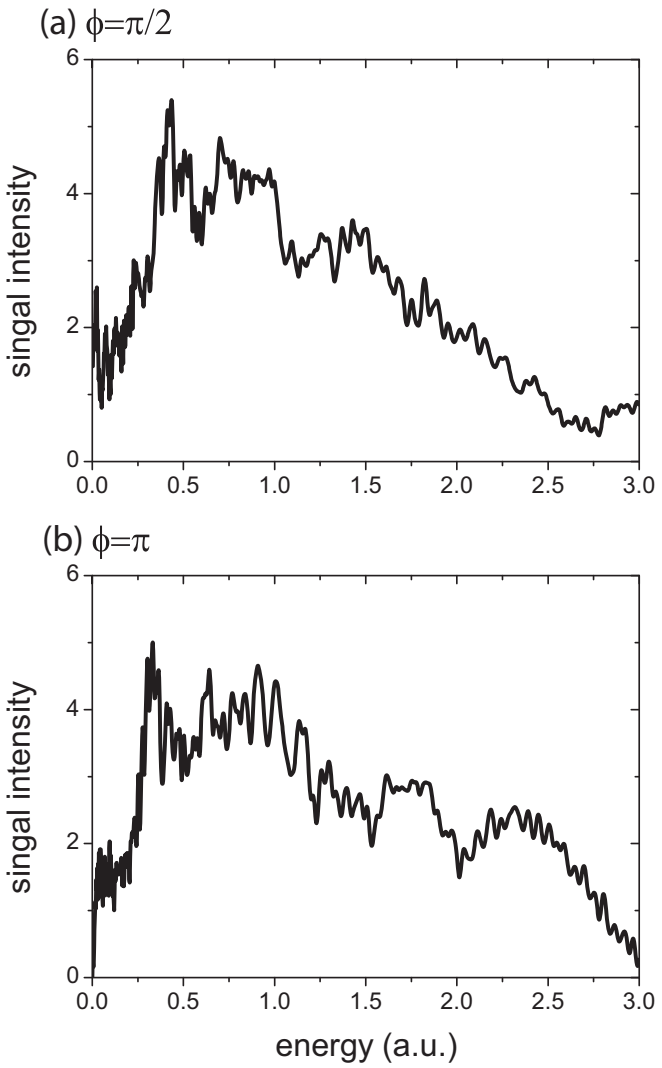

FIG. 6. ATI energy spectra in the molecule H_2^+ aligned along the x axis by four-color circularly polarized laser pulses at frequencies $\omega_1 = \omega_0, \omega_2 = 3\omega_0, \omega_3 = 2\omega_0$, and $\omega_4 = 4\omega_0$, where $\omega_0 = 0.057$ a.u. corresponding to $\lambda_0 = 800$ nm. The CEPs of pulses are (a) $\phi = \pi/2$, i.e., $\phi_1 = \phi_2 = 0$ and $\phi_3 = \phi_4 = \pi/2$, and (b) $\phi = \pi$, i.e., $\phi_1 = \phi_2 = 0$ and $\phi_3 = \phi_4 = \pi$. The intensity and duration of pulses are $I_0 = 2\times10^{14}$ W/cm^2 ($E_0 = 0.0755$ a.u.) and $T = 21.15$ fs. Arbitrary units in ATI energy spectra are used.

geometry and orientation [60], which allows us to retrieve the molecular orbital.

IV. CONCLUSIONS

We have studied molecular ATI processes in aligned H_2^+ by using multiple-frequency circularly polarized laser fields. Photoionization obtained from numerical solutions of corresponding TDSEs shows that ATI spectra exhibit maximum cutoff energies which depend on the frequency combinations of pulses. We first consider bichromatic ω_1 and ω_2 circular polarization processes with co- and counter-rotating components. It is found that, for counter-rotating cases, the maximum $2U_p$ cutoff occurs, where the ponderomotive energy $U_p = (2E_0)^2/4\omega^2$ with the average frequency $\omega = (\omega_1 + \omega_2)/2$. However, for corotating cases, the cutoff of ATI spectra is suppressed, which is attributed to the strong effects of the Coriolis force in a rotating frame with frequency $\bar{\omega} = (\omega_1 - \omega_2)/2$, larger than ω. The angular ATI spectra correspond to the photoionization trajectories, illustrating the symmetry of the net laser field. We also present four-color ATI processes. In the rotating frame, the field-molecule Hamiltonian corresponds to a bichromatic linear polarization process. The pulse modulation thus leads to an extension of ATI spectra.

The present demonstration in principle paves the way to control ultrafast electron dynamics by multiple-frequency circularly polarized laser pulses. The dependence of the photoelectron trajectories on the frequency combination and helicity of ionizing laser pulses allows us to characterize the property of laser pulses and probe atomic and molecular structure by photoelectron holography [19,20]. Although a simple single-electron molecular ion H_2^+ is used, similar electron dynamics phenomena should be predicted in more complex molecules [36,45,61,62], thus opening an opportunity for structure determination of molecules from the measurements of ATI processes.

ACKNOWLEDGMENT

The authors thank RQCHP and Compute Canada for access to massively parallel computer clusters and NSERC, FQRNT for support of this research.

[1] T. Brabec and F. Krausz, Rev. Mod. Phys. **72**, 545 (2000).
[2] F. Krausz and M. Ivanov, Rev. Mod. Phys. **81**, 163 (2009).
[3] S. Chelkowski, P. B. Corkum, and A. D. Bandrauk, Phys. Rev. Lett. **82**, 3416 (1999).
[4] P. Ma, C. Wang, S. Luo, X. Yu, X. Li, Z. Wang, W. Hu, J. Yu, Y. Yang, X. Tian, Z. Cui, and D. Ding, J. Phys. B: At. Mol. Opt. Phys. **51**, 094002 (2018).
[5] T. Zuo, A. D. Bandrauk, and P. B. Corkum, Chem. Phys. Lett. **259**, 313 (1996).
[6] M. Meckel, D. Comtois, D. Zeidler, A. Staudte, D. Pavicic, H. C. Bandulet, H. Pepin, J. C. Kieffer, R. Dorner, D. M. Villeneuve, and P. B. Corkum, Science **320**, 1478 (2008).
[7] T. Morishita, A. T. Le, Z. Chen, and C. D. Lin, Phys. Rev. Lett. **100**, 013903 (2008).
[8] K. J. Schafer, B. Yang, L. F. DiMauro, and K. C. Kulander, Phys. Rev. Lett. **70**, 1599 (1993).
[9] P. B. Corkum, Phys. Rev. Lett. **71**, 1994 (1993).
[10] P. Agostini, F. Fabre, G. Mainfray, G. Petite, and N. K. Rahman, Phys. Rev. Lett. **42**, 1127 (1979).
[11] P. B. Corkum, N. H. Burnett, and F. Brunel, Phys. Rev. Lett. **62**, 1259 (1989).
[12] W. Becker, F. Grasbon, R. Kopold, D. B. Milošević, G. G. Paulus, and H. Walther, Adv. At. Mol. Phys. **48**, 35 (2002).
[13] D. B. Milošević, G. G. Paulus, D. Bauer, and W. Becker, J. Phys. B: At. Mol. Opt. Phys. **39**, R203 (2006).
[14] C. D. Lin, A.-T. Le, Z. Chen, T. Morishita, and R. Lucchese, J. Phys. B: At. Mol. Opt. Phys. **43**, 122001 (2010).
[15] P. Agostini and L. F. DiMauro, Adv. At. Mol. Opt. Phys. **61**, 117 (2012).
[16] G. G. Paulus, W. Nicklich, H. Xu, P. Lambropoulos, and H. Walther, Phys. Rev. Lett. **72**, 2851 (1994).
[17] K. L. LaGattuta and J. S. Cohen, J. Phys. B: At. Mol. Opt. Phys. **31**, 5281 (1998).
[18] M. Peters, T. T. Nguyen-Dang, E. Charron, A. Keller, and O. Atabek, Phys. Rev. A **85**, 053417 (2012).
[19] Y. Huismans *et al.*, Science **331**, 61 (2011).
[20] X. B. Bian, Y. Huismans, O. Smirnova, K. J. Yuan, M. J. J. Vrakking, and A. D. Bandrauk, Phys. Rev. A **84**, 043420 (2011).
[21] K. J. Yuan and A. D. Bandrauk, Phys. Rev. A **84**, 013426 (2011).
[22] W. Yang, Z. Sheng, X. Feng, M. Wu, Z. Chen, and X. Song, Opt. Express **22**, 2519 (2014).
[23] E. Hasovic, W. Becker, and D. B. Milošević, Opt. Express **24**, 6413 (2016).
[24] C. A. Mancuso, D. D. Hickstein, P. Grychtol, R. Knut, O. Kfir, X.-M. Tong, F. Dollar, D. Zusin, M. Gopalakrishnan, C. Gentry, E. Turgut, J. L. Ellis, M.-C. Chen, A. Fleischer, O. Cohen, H. C. Kapteyn, and M. M. Murnane, Phys. Rev. A **91**, 031402(R) (2015).
[25] C. A. Mancuso, D. D. Hickstein, K. M. Dorney, J. L. Ellis, E. Hasovic, R. Knut, P. Grychtol, C. Gentry, M. Gopalakrishnan, D. Zusin, F. J. Dollar, X.-M. Tong, D. B. Milošević, W. Becker, H. C. Kapteyn, and M. M. Murnane, Phys. Rev. A **93**, 053406 (2016).
[26] T. Zuo and A. D. Bandrauk, J. Nonlinear Opt. Phys. Mater. **04**, 533 (1995).
[27] A. D. Bandrauk and H. Z. Lu, Phys. Rev. A **68**, 043408 (2003).
[28] S. Long, W. Becker, and J. K. McIver, Phys. Rev. A **52**, 2262 (1995).
[29] D. B. Milošević, W. Becker, and R. Kopold, Phys. Rev. A **61**, 063403 (2000).
[30] K. J. Yuan and A. D. Bandrauk, Phys. Rev. Lett. **110**, 023003 (2013); J. Phys. B **45**, 074001 (2012).
[31] F. Mauger, A. D. Bandrauk, and T. Uzer, J. Phys. B **49**, 10LT01 (2016); A. D. Bandrauk, F. Mauger, and K. J. Yuan, *ibid.* **49**, 23LT01 (2016).
[32] A. Fleischer, O. Kfir, T. Diskin, P. Sidorenko, and O. Cohen, Nat. Photon. **8**, 543 (2014).
[33] O. Kfi, P. Grychtol, E. Turgut, R. Knut, D. Zusin, D. Popmintchev, T. Popmintchev, H. Nembach, J. M. Shaw, A. Fleischer, H. Kapteyn, M. Murnane, and O. Cohen, Nat. Photon. **9**, 99 (2015).

[34] T. Fan, P. Grychtol, R. Knut, C. Hernandez-Garcia, D. D. Hickstein, D. Zusin, C. Gentry, F. J. Dollar, C. A. Mancuso, C. W. Hogle,O. Kfir, D. Legut, K. Carva, J. L. Ellis, K. M. Dorney, C. Chen, O. G. Shpyrko, E. E. Fullerton, O. Cohen, P. M. Oppeneer *et al.*, Proc. Natl. Acad. Sci. USA **112**, 14206 (2015).
[35] D. B. Milošević, Phys. Rev. A **92**, 043827 (2015); Opt. Lett. **40**, 2381 (2015).
[36] D. Baykusheva, M. S. Ahsan, N. Lin, and H. J. Wörner, Phys. Rev. Lett. **116**, 123001 (2016).
[37] L. Medisauskas, J. Wragg, H. van der Hart, and M. Y. Ivanov, Phys. Rev. Lett. **115**, 153001 (2015).
[38] M. Li, W.-C. Jiang, H. Xie, S. Luo, Y. Zhou, and P. Lu, Phys. Rev. A **97**, 023415 (2018).
[39] J. M. Ngoko Djiokap, S. X. Hu, L. B. Madsen, N. L. Manakov, A. V. Meremianin, and A. F. Starace, Phys. Rev. Lett. **115**, 113004 (2015).
[40] J. M. Ngoko Djiokap, A. V. Meremianin, N. L. Manakov, S. X. Hu, L. B. Madsen, and A. F. Starace, Phys. Rev. A **96**, 013405 (2017).
[41] K.-J. Yuan, S. Chelkowski, and A. D. Bandrauk, Phys. Rev. A **93**, 053425 (2016); K.-J. Yuan, H. Lu, and A. D. Bandrauk, J. Phys. B: At. Mol. Opt. Phys. **50**, 124004 (2017).
[42] D. Pengel, S. Kerbstadt, D. Johannmeyer, L. Englert, T. Bayer, and M. Wollenhaupt, Phys. Rev. Lett. **118**, 053003 (2017).
[43] D. Pengel, S. Kerbstadt, L. Englert, T. Bayer, and M. Wollenhaupt, Phys. Rev. A **96**, 043426 (2017).
[44] K.-J. Yuan and A. D. Bandrauk, Phys. Rev. A **92**, 063401 (2015); A. D. Bandrauk, J. Guo, and K. J. Yuan, J. Opt. (Bristol, UK) **19**, 124016 (2017).
[45] S. Beaulieu, A. Comby, D. Descamps, B. Fabre, G. A. Garcia, R. Geneaux, A. G. Harvey, F. Legare, Z. Masin, L. Nahon, A. F. Ordonez, S. Petit, B. Pons, Y. Mairesse, O. Smirnova, and V. Blanchet, Nat. Phys. **14**, 484 (2018).
[46] D. Ayuso, P. Decleva, S. Patchkovskii, and O. Smirnova, J. Phys. B: At. Mol. Opt. Phys. **51**, 06LT01 (2018); **51**, 124002 (2018).
[47] O. Neufeld and O. Cohen, Phys. Rev. Lett. **120**, 133206 (2018).
[48] M. V. Frolov, N. L. Manakov, and A. F. Starace, Phys. Rev. A **79**, 033406 (2009).
[49] A. D. Bandrauk and H. Z. Lu, Phys. Rev. A **72**, 023408 (2005).
[50] A. D. Bandrauk and H. Shen, J. Chem. Phys. **99**, 1185 (1993).
[51] K. J. Yuan, H. Z. Lu, and A. D. Bandrauk, Phys. Rev. A **83**, 043418 (2011).
[52] H. Ibrahim, C. Lefebvre, A. D. Bandrauk, A. Staudte, and F. Légaré, J. Phys. B: At. Mol. Opt. Phys. **51**, 042002 (2018).
[53] D. M. Reich and L. B. Madsen, Phys. Rev. A **93**, 043411 (2016).
[54] K. J. Yuan and A. D. Bandrauk, Phys. Rev. A **97**, 023408 (2018); A. D. Bandrauk and K. J. Yuan, J. Phys. B: At. Mol. Opt. Phys. **51**, 074001 (2018).
[55] M. Lein, J. Phys. B: At. Mol. Opt. Phys. **40**, R135 (2007).
[56] C. Chen, Z. Tao, C. Hernandez-Garcia, P. Matyba, A. Carr, R. Knut, O. Kfir, D. Zusin, C. Gentry, P. Grychtol, O. Cohen, L. Plaja, A. Becker, A. Jaron-Becker, H. Kapteyn, and M. Murnane, Sci. Adv. **2**, e1501333 (2016).
[57] A. Gazibegović-Busuladžić, M. Busuladžić, E. Hasović, W. Becker, and D. B. Milošević, Phys. Rev. A **97**, 043432 (2018).
[58] Z. Zeng, Y. Cheng, X. Song, R. Li, and Z. Xu, Phys. Rev. Lett. **98**, 203901 (2007).
[59] D. Peng, L. W. Pi, M. V. Frolov, and A. F. Starace, Phys. Rev. A **95**, 033413 (2017).
[60] X. B. Bian and A. D. Bandrauk, Phys. Rev. Lett. **108**, 263003 (2012); Phys. Rev. A **89**, 033423 (2014).
[61] A. Comby, S. Beaulieu, M. Boggio-Pasqua, D. Descamps, F. Legare, L. Nahon, S. Petit, B. Pons, B. Fabre, Y. Mairesse, and V. Blanchet, J. Phys. Chem. Lett. **7**, 4514 (2016).
[62] S. Beaulieu, A. Comby, A. Clergerie, J. Caillat, D. Descamps, N. Dudovich, B. Fabre, R. Geneaux, F. Legare, S. Petit, B. Pons, G. Porat, T. Ruchon, R. Taieb, V. Blanchet, and Y. Mairesse, Science **358**, 1288 (2017).